



Edge-engineered self-assembled hierarchical plasmonic SERS templates

N. Pliatsikas^{a,*}, N. Kalfagiannis^{b,*}, J. Arvanitidis^a, D. Christofilos^c, D.C. Koutsogeorgis^b,
A. Kagkoura^d, K. Sefiane^d, V. Koutsos^d, P. Patsalas^a

^a Department of Physics, Aristotle University of Thessaloniki, Thessaloniki GR-54124, Greece

^b School of Science and Technology, Nottingham Trent University, Nottingham, Northern Ireland NG11 8NS, United Kingdom

^c School of Chemical Engineering and Physics Laboratory, Faculty of Engineering, Aristotle University of Thessaloniki, Thessaloniki GR-54124, Greece

^d School of Engineering, The University of Edinburgh, King's Buildings, Edinburgh EH9 3FB, United Kingdom

ARTICLE INFO

Keywords:

Surface enhanced Raman scattering (SERS)
Plasmonic nanostructures
Self-assembled nanostructures
Laser annealing
Wettability

ABSTRACT

Surface enhanced Raman scattering (SERS) has emerged as a reliable and ultra-sensitive sensing technique used in analytical diagnostics, forensics, and biomedical applications. Although SERS may be sensitive enough to detect single molecules, such extreme performance is achieved with sophisticated and complex nanostructure designs that are hard to implement on an industrial scale. This work presents an understanding of the plasmonic and wetting phenomena taking place on Ag nanoparticles (supported on Si) produced by laser annealing and dewetting of sputtered ultra-thin layers enabling the fast (<3 min), scalable and cost-effective production of SERS templates with a hierarchical plasmonic structure. In particular, the produced SERS templates incorporate micron-scale accumulation spots of the Rhodamine 6 G test molecules, superimposed over nano-scale hot spots, where electric near field enhancement occurs due to plasmon resonances. This combination increases drastically the SERS signal, making it suitable for fast chemical diagnostics.

Introduction

Surface enhanced Raman scattering (SERS) is a non-invasive spectroscopic technique that exploits unique molecular vibrational modes as fingerprints to identify and quantify analytes [1–6]. To promote Raman signal, which is inherently low [7], SERS employs metallic nanostructures, where collective oscillations of the metal's conduction electrons, the so called localized surface plasmon resonance (LSPR) occur upon appropriate optical excitation. LSPR magnifies the electric field at the vicinity of the nanoparticles, thus enhancing the radiation-molecule interaction and the Raman scattering signal. SERS has been used for rapid, highly sensitive and ultra-trace analysis in many fields such as chemistry, biology, medicine, pharmacology, forensics and life science [8–16]. In order to obtain SERS-active templates, it is necessary to consider the template surface properties and morphology. Recently, the scientific interest has concentrated on increasing the sensitivity of SERS to broaden its applicability by introducing hydrophobic and superhydrophobic materials into the SERS field as a method for enrichment of the analyte [17–24].

The combination of SERS and hydrophobic surfaces can enhance considerably the detection limit of Raman response [25–31]. When a

solution is poured onto the hydrophobic substrate, the highly diluted solute will be concentrated and localized into a very small region of the substrate, where plasmonic near field hot spots are used to carry out molecule detection; evidently, the distribution of dried solute molecules is essential for the enhancement of SERS sensitivity. Hydrophobic and superhydrophobic SERS micro/nano-structured substrates are principally developed by lithographic techniques, electron or ion beam etching, electrochemical deposition, *etc.* and it is possible to attain a low detection limit, down to 10^{-18} M [26–28,32,33]. Most of these methods are either complicated or time-consuming, so a simple way to fabricate hydrophobic substrates with a high throughput and at macroscopic scale is still highly sought after. Laser annealing (LA) is one of the most promising tools for simple, high efficiency, fast processing, scalable and controllable micro and nano surface structuring due to its high peak power and ultrashort irradiation duration [34–38]. Varying the LA conditions allows for the fabrication of Ag nanoparticles (NPs) with a variety of morphologies and sizes available [34–39], not only for various sensing applications but also as building blocks for further fabrication of nano and microstructures. Apart from NPs, other forms of plasmonic nanostructures produced by physical methods have been suggested in the literature, such as nanoneedles arrays [40,41], nanorods arrays [42],

* Corresponding authors.

E-mail addresses: nipliats@physics.auth.gr (N. Pliatsikas), nikolaos.kalfagiannis@ntu.ac.uk (N. Kalfagiannis).

<https://doi.org/10.1016/j.apsadv.2021.100186>

Received 30 June 2021; Received in revised form 6 October 2021; Accepted 11 October 2021

Available online 20 October 2021

2666-5239/© 2021 The Author(s). Published by Elsevier B.V. This is an open access article under the CC BY license (<http://creativecommons.org/licenses/by/4.0/>).

and nanopores [43].

In this work, we produced pre-determined patterns of metal nanostructures in a highly selective, ultra-fast and high-throughput fashion employing LA. We controlled the morphology and size distribution by changing crucial LA parameters such as the applied laser wavelength, the number of pulses, the energy density of each pulse (fluence) and the micron-scale area selective processing (patterning) of the LA spot through a macroscopic optical mask. The laser-processed metallic nanostructures were utilized as SERS templates *via* drop-casting of aqueous solutions of Rhodamine 6G (R6G), a widely used probe molecule exploited as a standard for the assessment of SERS substrates, and subsequently, their optical, chemical, wetting, and structural properties were studied in an effort to find the parameters that affect the efficiency of chemical sensing. We provide here solid evidence on the effects of nanoparticle morphology and size distribution on the hydrophobicity of the plasmonic templates and the SERS performance. An intriguing result was that edges created by the patterned laser spot used for LA have a notable influence on the SERS signal. Based on this, we designed and fabricated hierarchical plasmonic structures that feature an underlying pattern of plasmonic nanoparticles superimposed onto a micron scale motif, which have a far-reaching effect on the SERS signal.

Experimental part

A schematic illustration of the experimental steps carried out in this work is presented in Fig. 1.

Preparation of SERS templates

Ultra-thin Ag films (10 nm nominal thickness) were deposited via RF-Magnetron Sputtering (Fig. 1a) in a high vacuum chamber on commercial, Czochralski-grown, n-type Si(100) wafers, with a 2 nm native oxide layer. In order to create plasmonic silver nanostructures, a laser annealing (LA) process was employed, as shown in Fig. 1b, according to Kalfagiannis et al. [34] This method is utilized to reproducibly fabricate nanoparticle (NP) templates at large scale. LA was carried out with a KrF excimer laser (pulse duration of 25 ns) emitting light at 248 nm. The laser pulses (1 and 15) were delivered to the sample at 1 Hz repetition rate. The number of pulses was carefully chosen to provide two extreme morphological features *i.e.* large-size broad Gaussian distributions at 1 pulse and narrow Gaussian distributions at 15 pulses (see Ref. [34]). The laser fluence was varied from 350 to 800 mJ/cm² with a step of 150 mJ/cm². The beam delivery system comprised a variable attenuator (with a partially reflective first plate and a second plate that compensates for the parallel displacement of the beam caused by the first plate), a beam homogenizer (with two lens arrays and a condenser lens, which provide a top-hat profile on both axes), a stage for interchangeable masks for selecting various laser spot shapes onto the sample and a combination of field and projection lenses that defined the size of the

mask shape onto the sample. The samples were mounted on an X–Y–Z translational stage. The LA beam delivered onto the samples was a 2.4 × 2.4 mm² square and it produced a homogeneous SERS template (*i.e.* with the same Ag NPs size distribution over the entire area) of the same area; additional SERS templates were produced with identical conditions but with employment of a mask that included micron-scale stripes in order to form the hierarchical structures.

SERS protocol

A proof-of-concept detection experiment was carried out using the common SERS molecule, Rhodamine 6G (R6G). Drop casting was utilized to apply a R6G droplet (~16 μL), 10 nM in water, onto the active surface of the plasmonic NP templates (Fig. 1c) and let dry at room temperature for 30 min. The 10 nM solution was selected in order to be close to the detection limit of SERS provided by Ag nanoparticles supported on Si, produced by thermal dewetting of sputtered Ag films, which can be as low as 1 nM [44]. The untreated Ag sputtered templates, which were used as signal base line, can hardly detect the 10 nM solution. All the SERS measurements were conducted from the middle area of the droplet stain (unless otherwise specified) in order to be consistent and follow a methodology which can be applied in any type of rapid testing templates.

The suitability of the plasmonic templates as SERS templates was evaluated by Raman Spectroscopy (Fig. 1d). The Raman spectra were recorded in the backscattering geometry using a microscope-equipped single stage spectrometer (LabRAM HR, Horiba) with a charge-coupled device (CCD) Peltier-cooled detector and excited using the 515 nm line of a solid-state laser or the 632.8 nm line of an He-Ne laser focused on the sample with a standard 100× microscope objective. The spectral resolution of the system was 3–3.5 cm⁻¹ depending on the excitation wavelength. The laser power on the sample was kept constant in all measurements (~2 μW). In order to avoid photobleaching effects, the effective laser intensity delivered on the sample was further reduced by taking advantage of the “macro” mode of the system (DuoScan™ Macro), where the laser spot is rapidly scanned over a 10 × 10 μm² sample area.

Surface characterization

The contact angle measurements were conducted by a Contact Angle Analyzer (FTÅ200, First Ten Ångstroms, Inc., Portsmouth). The templates were placed on an XY-axis workbench; a drop of deionized water of approximately 3 μL was generated by a pipette and gently deposited on the surface of the templates at room temperature. The measurements were repeated on different locations of the templates and averaged.

Imaging characterization of Ag NPs was performed using a JSM-7100F LV (JEOL UK) Field Emission Gun Scanning Electron Microscope (FEG-SEM), at an operating voltage of 10–15 kV and a working

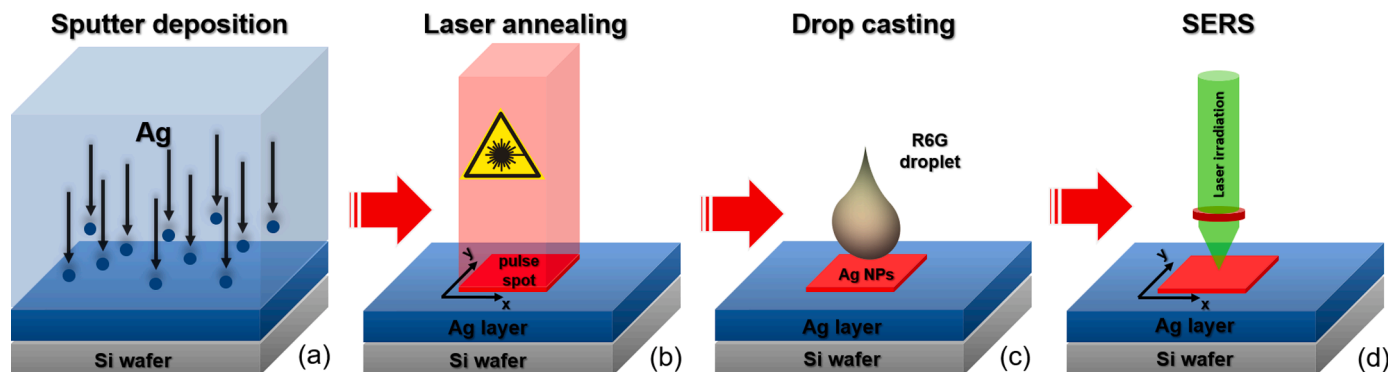


Fig. 1. Schematic representation of the processing steps in the present work: (a) sputter deposition of ultrathin silver layers, (b) dewetting of silver by laser annealing to form supported plasmonic NPs, (c) drop casting of a R6G aqueous solution (10 nM), (d) Raman measurements.

distance of 10.4–10.6 mm. SEM images were analyzed using the ImageJ software package [45], to determine the fraction of the substrate covered by the Ag NPs after the LA process.

X-ray photoelectron spectroscopy (XPS) was performed to identify the surface chemistry of the templates using an Axis Ultra DLD system by Kratos Analytical equipped with a monochromated Al-K α X-ray beam, a hemispherical sector analyzer and a multichannel detector. A pass energy of 20 eV has used while the spectra calibrated by considering C-1 s peak (originating from carbon surface contamination) to be located at 284.6 eV.

Results and discussion

The surface morphology of the SERS templates produced by LA was evaluated by SEM (Fig. 2). Note that no significant changes to the surface chemistry of the Ag NPs is detected after laser annealing processing as evident by XPS measurements performed on the plasmonic templates (Fig. S1 of the online supporting information).

SERS testing of the templates took place at room temperature and after drop-casting and drying of a droplet of a 10 nM aqueous R6G

solution. A 632.8 nm laser beam was selected for excitation of the Raman spectra in order to avoid background in the signal due to fluorescence emission of R6G [46]; additional Raman spectra using a 515 nm excitation beam did not result in qualitatively different results. The liquid droplet dried in a ring-shaped stain, a phenomenon known in the literature as coffee stain (or coffee ring) effect [47–49]. The SERS spectra of the dried R6G showed sharp peaks within the examined region (between 550 and 1700 cm^{-1}), that were identified from known spectra in the literature [50,51] (see online supporting information - Fig. S2 and Table S1); the stronger peaks are located at 610, 770, and 1650 cm^{-1} . In Fig. 3a,b, we present the SERS spectra obtained after Raman measurements of R6G solution on plasmonic templates with Ag NPs that have been fabricated by LA at a laser fluence varying from 350 mJ/cm^2 up to 800 mJ/cm^2 with a step of 150 mJ/cm^2 , in order to achieve a diverse population of plasmonic nanoparticles [34]. The underlying plasmonic NPs were formed by LA with 1 pulse (Fig. 3a) and 15 pulses (Fig. 3b). In particular, the utilization of 15 pulses revealed strong LSPR in the visible spectral range, while in the case of 1 pulse, LSPR appears in two distinct frequencies due to the bi-modal size distribution (Fig. 2).

In order to quantify the SERS signal, the total integrated intensity of the three dominant Raman peaks of R6G at 610, 770, and 1650 cm^{-1} was obtained by their fitting with Lorentzian curves. These peaks are assigned to the C—C—C ring mode, the C—H out of plane bending mode and the aromatic C—C stretching mode, respectively [44,50,51]. The results are shown in Fig. 3c. For both the cases of 1 and 15 laser pulses, the SERS signal increases linearly for increasing LA fluence from 350 mJ/cm^2 to 650 mJ/cm^2 , where the maximum is observed. Beyond that fluence threshold, there is a sharp drop in the SERS signal, which is accompanied by reduction of the Si surface coverage by Ag (Fig. 3d, with data determined from the SEM images illustrated in Fig. 2) and by the reduction of water contact angle (WCA), Fig. 3e. More specifically, SEM revealed a systematic increase of the Ag surface coverage upon increasing fluence, due to the NPs becoming smaller and more close-packed, and furthermore, a faceted morphology of the NPs that has been reported to enhance the SERS performance in Au NPs [52]. On the other hand, further increasing the fluence to 800 mJ/cm^2 causes a moderate reduction of the Ag coverage due to ablation.

The variations of the WCA on the various SERS templates produced in this work are presented in Fig. 3e. The tangent method was used to calculate the contact angle, where we notice an increase in the angle/hydrophobicity, approaching its maximum value at the LA fluence of 650 mJ/cm^2 for both 1 and 15 pulses. Identically to the SERS signal behavior, a sharp decrease of the WCA occurs at the fluence of 800 mJ/cm^2 ; the effect being more pronounced for the case of 15 pulses due to the ablation of the NPs. Notably, the hydrophobicity correlates with the SERS signal, most probably due to affecting the accumulation of the R6G during the drying process. As we shall see below, it is very important to look at the mechanisms that affect SERS in order to further enhance its signal.

From the overall quantitative analysis, we can argue that the 15 pulses at 650 mJ/cm^2 LA fluence optimize the SERS performance of the presented Ag NP templates due to a combination of factors such as: (i) a more intense and narrower LSPR due to narrower size distribution of the plasmonic Ag NPs (Fig. S3), (ii) close-packing and increased density of the Ag NPs on the surface of the templates, as well as their faceting (Figs. 1 and 3d), resulting in the multiplication of efficient hot spots that provide improved near-field enhancement, and (iii) an improved hydrophobicity of the template ($\text{WCA} > 100^\circ$) (Fig. 3e) that resulted in the accumulation of the dried R6G molecules to smaller areas.

So far, we have examined the SERS signal inside the homogeneous LA-treated template region (laser spot size of $2.4 \times 2.4 \text{ mm}^2$), away from the edges. However, it appears that edge effects exhibit promising characteristics for the enhancement of the SERS signal. Fig. 4a, illustrates measurements of the SERS R6G signal in a line scan across a spot edge for a LA-treated template, stretching areas outside (untreated Ag

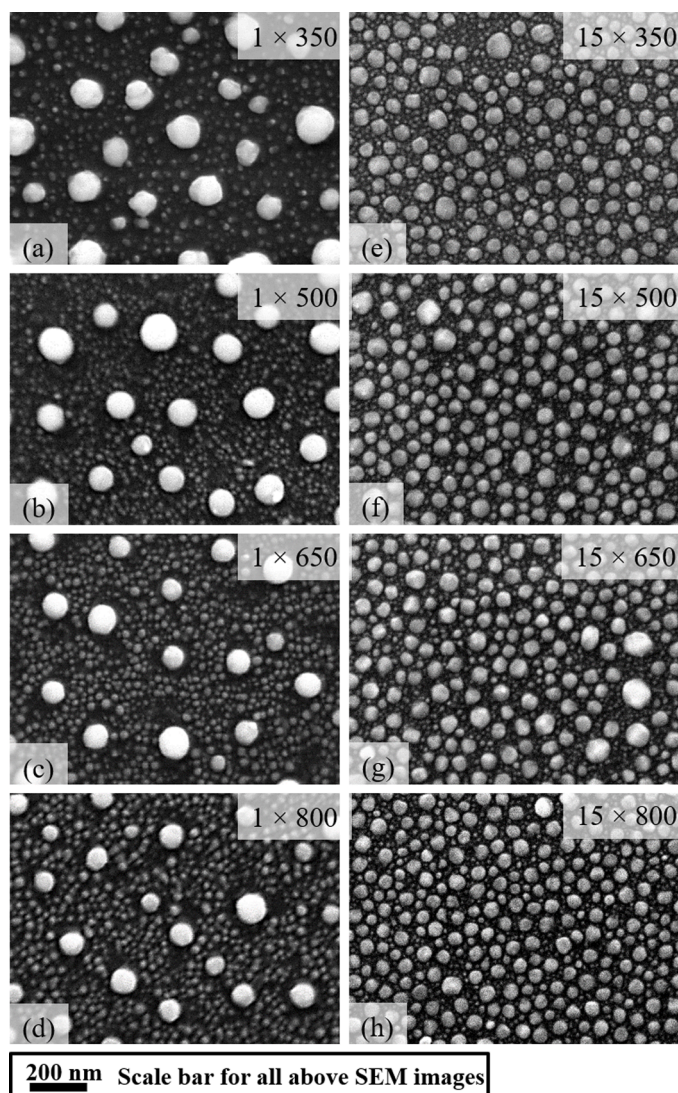


Fig. 2. SEM images of the surfaces of the Ag NP SERS templates produced by LA and used in this work, (a) 1 pulse at 350 mJ/cm^2 ; (b) 1 pulse at 500 mJ/cm^2 ; (c) 1 pulse at 650 mJ/cm^2 ; (d) 1 pulse at 800 mJ/cm^2 ; (e) 15 pulses at 350 mJ/cm^2 ; (f) 15 pulses at 500 mJ/cm^2 ; (g) 15 pulses at 650 mJ/cm^2 ; (h) 15 pulses at 800 mJ/cm^2 .

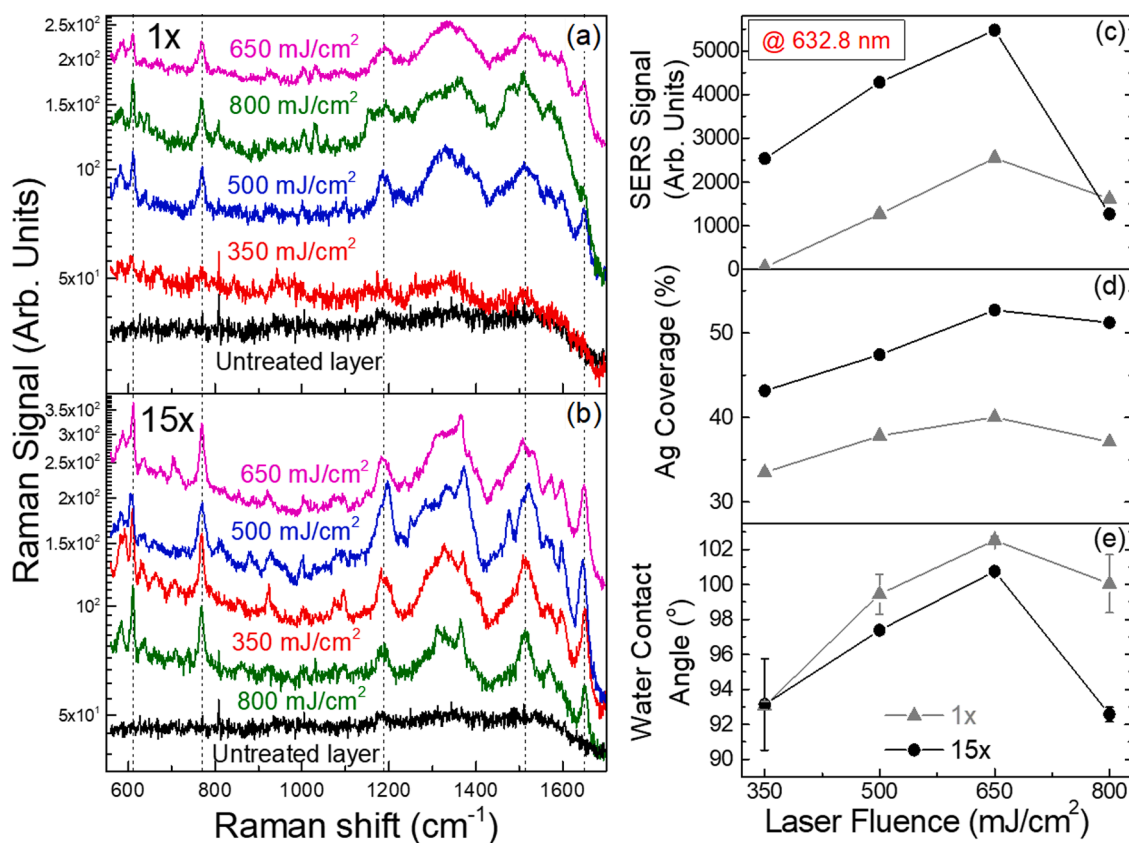


Fig. 3. SERS raw spectra excited at 632.8 nm of 10 nM R6G drop-casted and dried on a variety of Ag NP templates produced by LA using (a) 1 laser pulse, or (b) 15 laser pulses; (c) SERS signal obtained from the dominant Raman peaks at 610, 770, and 1650 cm^{-1} ; (d) coverage of Si by Ag NPs calculated from the SEM images; (e) water contact angle measurements performed at room temperature for 1 and 15 pulses.

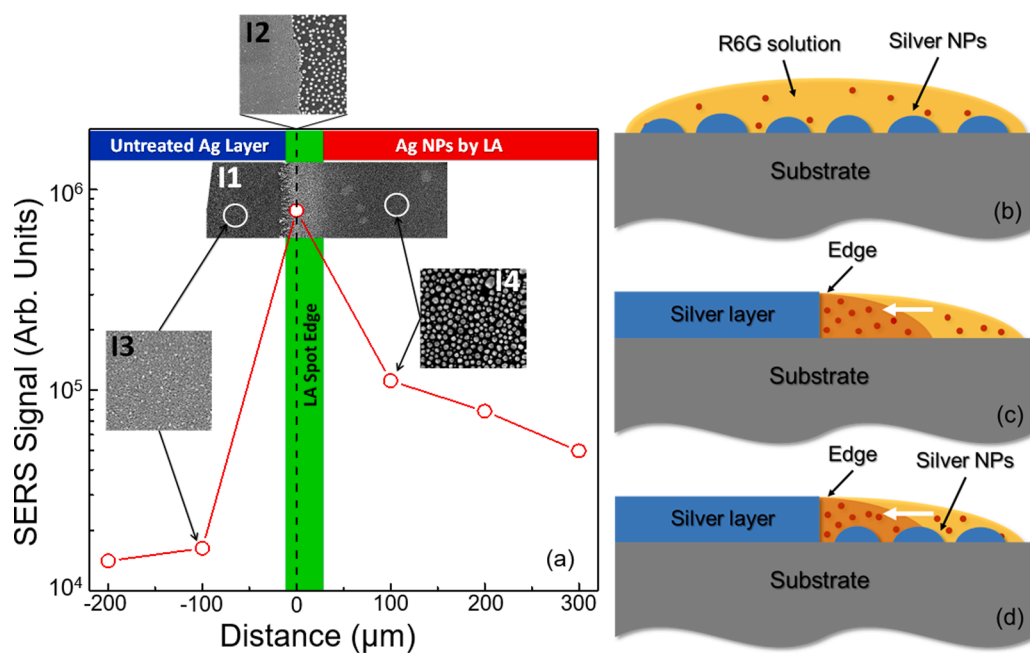


Fig. 4. (a) Line scan measurement of the SERS signal across a spot edge for a Ag NPs template fabricated by a single laser pulse at a fluence of 650 mJ/cm^2 . SERS signal from outside (untreated Ag sputtered), on the edge, and inside the LA-treated area (NPs) is illustrated. Inset 1 (I1) shows the accumulation of R6G at the edge of the laser spot (bright stripe), while Inset 2 (I2) shows, in higher magnification, the morphology of the boundary between the untreated sputtered Ag layer and the LA-treated part of the substrate (Ag NPs). Insets 3 and 4 (I3, I4) show the morphology of untreated and LA-treated areas further away from the edge. Schematic illustration of the wetting process of the R6G solution: (b) on Ag plasmonic NPs formed by the LA process (Nano-scale Enhancement), (c) at the vicinity of the edge of Ag thin layer without any Ag NPs (Micron-scale Enhancement), and (d) at the vicinity of the edge between the Ag layer and Ag plasmonic NPs (Nano- and Micron-scale Enhancement).

sputtered) and inside the LA-treated area (NPs). Quantification of the SERS signal is based, as previously, on the three stronger lines of R6G from the micro-Raman spectra presented in Fig. S4 of the online supporting information. In the untreated area (with sputter coated Ag), the

SERS signal is lower. On the other hand, within the LA-treated area (with Ag NPs), the SERS signal is about an order of magnitude higher due to the near-field enhancement around the Ag NPs formed by LA. However, the laser spot edge itself produced a SERS signal that was further

enhanced significantly (almost a further order of magnitude) due to a combination of the accumulation of R6G at the edge after drying (as shown in inset 1 in Fig. 4a) and the plasmonic nanoparticles at the vicinity to the edge being within the area probed in the micro-Raman measurements (inset 2 in Fig. 4a). As mentioned before, the coffee stain effect results in a ring with enriched particle/molecule density that forms when a colloidal droplet dries on a substrate in a pinned mode. According to Deegan et al. [47] this is due to the highest evaporation rate near the droplet's outer periphery that induces a capillary flow from the center of the droplet to the outer edge, leading to a higher density of particles/molecules at the edge than in the center. Furthermore, this effect can be enhanced via substrate roughness during the evaporation of colloidal droplets [53,54]. Additionally, Sharma et al. [55] studied a drying mechanism based on the coffee stain effect and managed to create cylindrical droplets using a parallel pattern of alternating hydrophobic and hydrophilic self-assembled monolayers. They also introduced a model to describe the transition from outward to inward flow creating edge density enriched particle patterns. In our case, we believe that the more hydrophobic regions (e.g., Ag NPs), repel the liquid towards the edges. This supports the consideration that the edges can act as selective accumulation spots attracting more R6G particles/molecules during the drying process, explaining the accumulation of R6G molecules at the LA spot edge (inset 2 in Fig. 4a).

This well-documented behavior can enable the improvement of the NP templates' performance by generating "accumulation edges" for the probed substance at the LA pulse edges between Ag layers and the Ag NP areas. Based on this, we can design templates that increase the SERS signal taking into account micron- and nano-scale structural approaches for the facile production of SERS templates via LA: (i) employ plasmonic NPs, taking advantage of the maximum near field enhancement at "hot spots" but with low solute concentration (Fig. 4b), (ii) create micron-scale structures to form "accumulation edges" exploiting the selective deposition of solute molecules at edges to maximize the solute concentration (after drying) but with no field enhancement (Fig. 4c), and (iii) combine the active "hot spots" around and between "accumulation edges" placing plasmonic NPs in the vicinity of micron-scale long structures (Fig. 4d), exploiting both the aforementioned benefits, thus providing the optimal SERS performance.

Taking advantage of the above, a projection mask was used during the LA process to create a hierarchical structure with multiple dimensions and functions: micron-scale grids that increase dramatically the length of accumulation edges, and nano-scale plasmonic particles that create hot spots for SERS. In particular, an optical mask in the laser beam delivery system was used, which is capable of creating lines of 100 μm width and 200 μm spacing, to increase the accumulation edges. For this demonstration, the laser conditions were a single pulse with 650 mJ/cm^2 laser fluence (which constitute the best case of Fig. 3 for 1 laser pulse). Also, the Raman excitation wavelength was 515 nm in order to better overlap with the LSPR of the plasmonic NPs and the molecular resonance from the analyte [46,50,56–58]. In addition, the structural features encountered on the sample are now of the order of 100 μm , therefore the "macro" mode of Raman system was employed and scanned an area of $80 \times 80 \mu\text{m}^2$ by the edge to prevent the photobleaching effect, as described previously.

Indeed, the simple stripes pattern (Fig. 5a, red solid line) revealed more intense and fine peaks of the SERS spectra of R6G, compared to the uniform square spot (Fig. 5a, black solid line). In a subsequent step, the projection mask was rotated by 90° , irradiating the same spot with a second laser pulse to create a crossed-stripes pattern (grid) for further increasing the accumulation of the edges. The SERS spectra recorded from the crossed-stripes pattern (Fig. 5a, blue solid line) appeared even further enhanced. The insets in Fig. 5b are optical microscopy images of each individual micron-scale pattern that resulted after LA ($2.4 \times 2.4 \text{ mm}^2$ each). For the simple stripes pattern, the SERS signal is doubled, while for the crossed stripes pattern, the SERS signal is enhanced almost 6-fold, compared to the homogeneous square spot, proving the

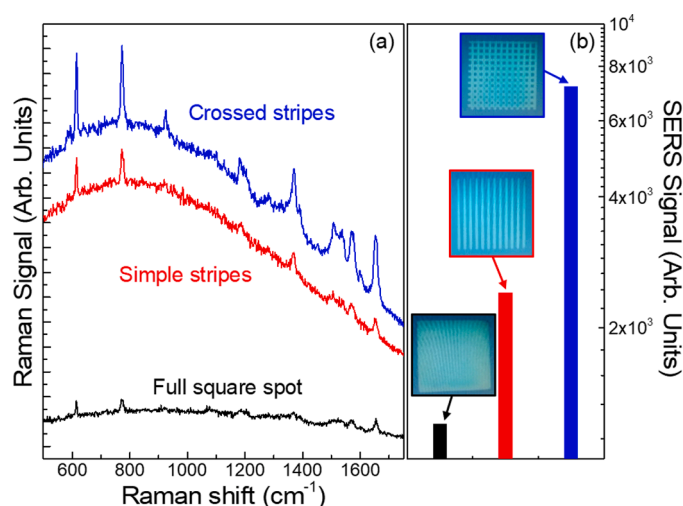


Fig. 5. (a) SERS spectra of 10 nM R6G drop-casted and dried on plasmonic templates developed after LA process. For LA, a single pulse operation at a 650 mJ/cm^2 fluence was selected, while predefined micron-scale patterns (stripes or grid) are formed on the substrate using a projection mask during the LA process. (b) Bar chart presenting the SERS signal for the full square spot (black bar) and the different micron-scale patterns; stripes (red bar) and grid (blue bar). (For interpretation of the references to color in this figure legend, the reader is referred to the web version of this article.)

effectiveness of the hierarchical patterning for SERS sensing. Based on Fig. 5b, the hierarchical pattern improves the SERS performance by almost an order of magnitude, by properly adjusting the laser annealing parameters (Fig. 3c).

Conclusions

Laser annealing of sputtered ultrathin silver layers is shown to be an effective tool for the fabrication of hierarchical SERS templates supported on Si, consisting of micron- and nano-scale features: extended edges and nanoparticles acting as accumulation edges and hot spots, respectively. The plasmonic performance and the hydrophobicity of the produced SERS templates are very sensitive to the laser annealing conditions (number of pulses and fluence). Upon careful selection of the NP size distribution, shape (faceting), and hydrophobicity, and the combination of micron-scale accumulation edges and nano-scale hot spots, the SERS performance can be improved as much as two orders of magnitude. This improvement potentially indicates that the detection limit of SERS by Ag NPs supported simply on Si, could be extended below the nM range, using a very fast (< 3 min for sputter deposition and less than 2 s for laser annealing), scalable, lithography-free, repeatable, and cost-effective process.

Funding sources

N. Kalfagiannis acknowledges funding from People Programme (Marie Curie Actions) LASER-PLASMON of the European Union's Seventh Framework Programme (FP7/2007–2013) under REA grant agreement no. PIEF-GA-2012–330,444.

CRedit authorship contribution statement

N. Pliatsikas: Writing – original draft. N. Kalfagiannis: Writing – original draft. J. Arvanitidis: Writing – original draft. D. Christofilos: Writing – original draft. D.C. Koutsogeorgis: Writing – original draft. A. Kagkoura: Writing – original draft. K. Sefiane: Writing – original draft. V. Koutsos: Writing – original draft. P. Patsalas: Writing – original draft.

Declaration of Competing Interest

The authors declare that they have no known competing financial interests or personal relationships that could have appeared to influence the work reported in this paper.

Acknowledgments

The authors would like to acknowledge Dr David Fairhurst, from Nottingham Trent University, for the fruitful discussions around the wetting of surfaces and his suggestions of interpreting the results of the single stripes and cross stripes plasmonic templates via the SERS experiments.

J.A., D.C. and P.P. acknowledge the Center for Interdisciplinary Research and Innovation of the Aristotle University of Thessaloniki (CIRI-AUTH) for the access to the Raman instrumentation.

Supplementary materials

Supplementary material associated with this article can be found, in the online version, at doi:10.1016/j.apsadv.2021.100186.

References

- J. Langer, D. Jimenez de Aberasturi, J. Aizpurua, R.A. Alvarez-Puebla, B. Auguie, J. Baumberg, G.C. Bazan, S.E.J. Bell, A. Boisen, A.G. Brolo, J. Choo, D. Ciialla-May, V. Deckert, L. Fabris, K. Faulds, F.J. Garcia de Abajo, R. Goodacre, D. Graham, A. J. Haes, C.L. Haynes, C. Huck, T. Itoh, M. Käll, J. Kneipp, N.A. Kotov, H. Kuang, E. C. Le Ru, H.K. Lee, J.F. Li, X.Y. Ling, S.A. Maier, T. Mayerhöfer, M. Moskovits, K. Murakoshi, J.M. Nam, S. Nie, Y. Ozaki, I. Pastoriza-Santos, J. Perez-Juste, J. Popp, A. Pucci, S. Reich, B. Ren, G.C. Schatz, T. Shegai, S. Schlucker, L.L. Tay, K. G. Thomas, Z.Q. Tian, R.P. Van Duyne, T. Vo-Dinh, Y. Wang, K.A. Willets, C. Xu, H. Xu, Y. Xu, Y.S. Yamamoto, B. Zhao, L.M. Liz-Marzán, Present and future of surface-enhanced Raman scattering, *ACS Nano* 14 (2020) 28–117, <https://doi.org/10.1021/acsnano.9b04224>.
- M. Fleischmann, P.J. Hendra, A.J. McQuillan, Raman spectra of pyridine adsorbed at a silver electrode, *Chem. Phys. Lett.* 26 (1974) 163–166, [https://doi.org/10.1016/0009-2614\(74\)85388-1](https://doi.org/10.1016/0009-2614(74)85388-1).
- D.L. Jeanmaire, R.P. Van Duyne, Surface Raman spectroelectrochemistry: part I. Heterocyclic, aromatic, and aliphatic amines adsorbed on the anodized silver electrode, *J. Electroanal. Chem.* 84 (1977) 1–20, [https://doi.org/10.1016/S0022-0728\(77\)80224-6](https://doi.org/10.1016/S0022-0728(77)80224-6).
- M.F. Cardinal, E. Vander Ende, R.A. Hackler, M.O. McAnally, P.C. Stair, G. C. Schatz, R.P. Van Duyne, Expanding applications of SERS through versatile nanomaterials engineering, *Chem. Soc. Rev.* 46 (2017) 3886–3903, <https://doi.org/10.1039/C7CS00207F>.
- A. Campion, P. Kambhampati, Surface-enhanced Raman scattering, *Chem. Soc. Rev.* 27 (1998) 241, <https://doi.org/10.1039/a827241z>.
- P.L. Stiles, J.A. Dieringer, N.C. Shah, R.P. Van Duyne, Surface-enhanced Raman spectroscopy, *Annu. Rev. Anal. Chem.* 1 (2008) 601–626, <https://doi.org/10.1146/annurev.anchem.1.031207.112814>.
- C. Kuttner, Plasmonics in sensing: from colorimetry to SERS analytics. *Plasmonics*, IntechOpen, 2018, <https://doi.org/10.5772/intechopen.79055>.
- C. Höppener, L. Novotny, Exploiting the light–metal interaction for biomolecular sensing and imaging, *Q. Rev. Biophys.* 45 (2012) 209–255, <https://doi.org/10.1017/S0033583512000042>.
- K. Kneipp, H. Kneipp, I. Itzkan, R.R. Dasari, M.S. Feld, Surface-enhanced Raman scattering: a new tool for biomedical spectroscopy, *Curr. Sci.* (1999).
- K. Hering, D. Ciialla, K. Ackermann, T. Dörfer, R. Möller, H. Schneidewind, R. Mattheis, W. Fritzsche, P. Rösch, J. Popp, SERS: a versatile tool in chemical and biochemical diagnostics, *Anal. Bioanal. Chem.* 390 (2008) 113–124, <https://doi.org/10.1007/s00216-007-1667-3>.
- M.D. Barnes, W.B. Whitten, J.M. Ramsay, Detecting single molecules in liquids, *Anal. Chem.* 67 (1995) 418A–423A, <https://doi.org/10.1021/ac00109a001>.
- K. Kneipp, Y. Wang, H. Kneipp, L.T. Perelman, I. Itzkan, R.R. Dasari, M.S. Feld, Single molecule detection using surface-enhanced Raman scattering (SERS), *Phys. Rev. Lett.* 78 (1997) 1667–1670, <https://doi.org/10.1103/PhysRevLett.78.1667>.
- T. Kang, S.M. Yoo, I. Yoon, S.Y. Lee, B. Kim, Patterned multiplex pathogen DNA detection by Au particle-on-wire SERS sensor, *Nano Lett.* 10 (2010) 1189–1193, <https://doi.org/10.1021/nl1000086>.
- D.A. Stuart, C.R. Yonzon, X. Zhang, O. Lyandres, N.C. Shah, M.R. Glucksberg, J. T. Walsh, R.P. Van Duyne, Glucose sensing using near-infrared surface-enhanced Raman spectroscopy: gold surfaces, 10-day stability, and improved accuracy, *Anal. Chem.* 77 (2005) 4013–4019, <https://doi.org/10.1021/ac0501238>.
- G. Braun, S.J. Lee, M. Dante, T.Q. Nguyen, M. Moskovits, N. Reich, Surface-enhanced Raman spectroscopy for DNA detection by nanoparticle assembly onto smooth metal films, *J. Am. Chem. Soc.* 129 (2007) 6378–6379, <https://doi.org/10.1021/ja070514z>.
- K.A. Willets, R.P. Van Duyne, Localized surface plasmon resonance spectroscopy and sensing, *Annu. Rev. Phys. Chem.* 58 (2007) 267–297, <https://doi.org/10.1146/annurev.physchem.58.032806.104607>.
- H. Kang, Y.J. Heo, D.J. Kim, J.H. Kim, T.Y. Jeon, S. Cho, H.M. So, W.S. Chang, S. H. Kim, Droplet-guiding superhydrophobic arrays of plasmonic microposts for molecular concentration and detection, *ACS Appl. Mater. Interfaces* 9 (2017) 37201–37209, <https://doi.org/10.1021/acsami.7b11506>.
- W.K. Wang, M.L. Zheng, W.Q. Chen, F. Jin, Y.Y. Cao, Z.S. Zhao, X.M. Duan, Microscale golden candock leaves self-aggregated on a polymer surface: Raman scattering enhancement and superhydrophobicity, *Langmuir* 27 (2011) 3249–3253, <https://doi.org/10.1021/la105145j>.
- T.Y. Jeon, J.H. Kim, S.G. Park, J.D. Kwon, D.H. Kim, S.H. Kim, Stacked-disk nanotower arrays for use as omniphobic surface-enhanced Raman scattering substrates, *Adv. Opt. Mater.* 4 (2016) 1893–1900, <https://doi.org/10.1002/adom.201600388>.
- S. Shin, J. Lee, S. Lee, H. Kim, J. Seo, D. Kim, J. Hong, S. Lee, T. Lee, A droplet-based high-throughput SERS platform on a droplet-guiding-track-engraved superhydrophobic substrate, *Small* 13 (2017), 1602865, <https://doi.org/10.1002/sml.201602865>.
- X. Li, H.K. Lee, I.Y. Phang, C.K. Lee, X.Y. Ling, Superhydrophobic-oleophobic Ag nanowire platform: an analyte-concentrating and quantitative aqueous and Organic toxin surface-enhanced Raman scattering sensor, *Anal. Chem.* 86 (2014) 10437–10444, <https://doi.org/10.1021/ac502955w>.
- R.A. Wallace, J.J. Charlton, T.B. Kirchner, N.V. Lavrik, P.G. Datskos, M. J. Sepaniak, Superhydrophobic analyte concentration utilizing colloid-pillar array SERS substrates, *Anal. Chem.* 86 (2014) 11819–11825, <https://doi.org/10.1021/ac5033947>.
- M. Cheung, W.W.Y. Lee, J.N. McCracken, I.A. Larmour, S. Brennan, S.E.J. Bell, Raman analysis of dilute aqueous samples by localized evaporation of submicroliter droplets on the tips of superhydrophobic copper wires, *Anal. Chem.* 88 (2016) 4541–4547, <https://doi.org/10.1021/acs.analchem.6b00563>.
- Z. Yu, W. Song, L. Chen, Y. Park, B. Zhao, Q. Cong, Y.M. Jung, Simple immersion to prepare a Zn/Ag biomimetic superhydrophobic surface and exploring its applications on SERS, *Colloids Surf. A Physicochem. Eng. Asp.* 467 (2015) 224–232, <https://doi.org/10.1016/j.colsurfa.2014.11.056>.
- Q. Tong, W. Wang, Y. Fan, L. Dong, Recent progressive preparations and applications of silver-based SERS substrates, *TrAC Trends Anal. Chem.* 106 (2018) 246–258, <https://doi.org/10.1016/j.trac.2018.06.018>.
- J.M. Rui Tan, J.J. Ruan, H.K. Lee, I.Y. Phang, X.Y. Ling, A large-scale superhydrophobic surface-enhanced Raman scattering (SERS) platform fabricated via capillary force lithography and assembly of Ag nanocubes for ultratrace molecular sensing, *Phys. Chem. Chem. Phys.* 16 (2014) 26983–26990, <https://doi.org/10.1039/C4CP03679D>.
- H.K. Lee, Y.H. Lee, Q. Zhang, I.Y. Phang, J.M.R. Tan, Y. Cui, X.Y. Ling, Superhydrophobic surface-enhanced Raman scattering platform fabricated by assembly of Ag nanocubes for trace molecular sensing, *ACS Appl. Mater. Interfaces* 5 (2013) 11409–11418, <https://doi.org/10.1021/am403655g>.
- F. De Angelis, F. Gentile, F. Mecarini, G. Das, M. Moretti, P. Candeloro, M. L. Coluccio, G. Cojoc, A. Accardo, C. Liberale, R.P. Zaccaria, G. Perozziello, L. Tirinato, A. Toma, G. Cuda, R. Cingolani, E. Di Fabrizio, Breaking the diffusion limit with super-hydrophobic delivery of molecules to plasmonic nanofocusing SERS structures, *Nat. Photonics* 5 (2011) 682–687, <https://doi.org/10.1038/nphoton.2011.222>.
- F. Gentile, M.L. Coluccio, R.P. Zaccaria, M. Francardi, G. Cojoc, G. Perozziello, R. Raimondo, P. Candeloro, E. Di Fabrizio, Selective on site separation and detection of molecules in diluted solutions with super-hydrophobic clusters of plasmonic nanoparticles, *Nanoscale* 6 (2014) 8208–8225, <https://doi.org/10.1039/C4NR00796D>.
- J. Wang, H. Luo, X. Song, X. Zu, J. Zhang, Y. Gu, G. Yi, Superhydrophobic Ag–Cu composite metal film as surface-enhanced Raman scattering substrate, *Nano* 13 (2018), 1850083, <https://doi.org/10.1142/S1793292018500832>.
- P. Fu, X. Shi, F. Jiang, X. Xu, Superhydrophobic nanostructured copper substrate as sensitive SERS platform prepared by femtosecond laser pulses, *Appl. Surf. Sci.* 501 (2020), 144269, <https://doi.org/10.1016/j.apsusc.2019.144269>.
- F. Gentile, M.L. Coluccio, N. Coppede, F. Mecarini, G. Das, C. Liberale, L. Tirinato, M. Leoncini, G. Perozziello, P. Candeloro, F. De Angelis, E. Di Fabrizio, Superhydrophobic surfaces as smart platforms for the analysis of diluted biological solutions, *ACS Appl. Mater. Interfaces* 4 (2012) 3213–3224, <https://doi.org/10.1021/am300556w>.
- X. He, Y. Liu, X. Xue, J. Liu, Y. Liu, Z. Li, Ultrasensitive detection of explosives via hydrophobic condensation effect on biomimetic SERS platforms, *J. Mater. Chem. C* 5 (2017) 12384–12392, <https://doi.org/10.1039/C7TC04325B>.
- N. Kalfagiannis, A. Siozios, D.V. Bellas, D. Toliopoulos, L. Bowen, N. Pliatsikas, W. M. Cranton, C. Kosmidis, D.C. Koutsogeorgis, E. Lidorikis, P. Patsalas, Selective modification of nanoparticle arrays by laser-induced self assembly (MONA-LISA): putting control into bottom-up plasmonic nanostructuring, *Nanoscale* 8 (2016) 8236–8244, <https://doi.org/10.1039/C5NR09192F>.
- N. Kalfagiannis, D.C. Koutsogeorgis, E. Lidorikis, P. Patsalas, Laser annealing as a platform for plasmonic nanostructuring. *Nanoplasmonics - Fundamentals Applications*, Intech, 2017, p. 29, <https://doi.org/10.5772/67670>.
- A. Siozios, D.C. Koutsogeorgis, E. Lidorikis, G.P. Dimitrakopoulos, T. Kehagias, H. Zoubos, P. Kominou, W.M. Cranton, C. Kosmidis, P. Patsalas, Optical encoding by plasmon-based patterning: hard and inorganic materials become photosensitive, *Nano Lett.* 12 (2012) 259–263, <https://doi.org/10.1021/nl2034738>.
- A. Siozios, H. Zoubos, N. Pliatsikas, D.C. Koutsogeorgis, G. Vourlias, E. Pavlidou, W. Cranton, P. Patsalas, Growth and annealing strategies to control the

- microstructure of AlN:Ag nanocomposite films for plasmonic applications, *Surf. Coat. Technol.* 255 (2014) 28–36, <https://doi.org/10.1016/j.surfcoat.2013.11.025>.
- [38] D.V. Bellas, D. Toliopoulos, N. Kalfagiannis, A. Siozios, P. Nikolaou, P.C. Kelires, D. C. Koutsogeorgis, P. Patsalas, E. Lidorikis, Simulating the opto-thermal processes involved in laser induced self-assembly of surface and sub-surface plasmonic nanostructuring, *Thin Solid Films* 630 (2017) 7–24, <https://doi.org/10.1016/j.tsf.2016.12.046>.
- [39] M.J. Beliatas, S.J. Henley, S.R.P. Silva, Engineering the plasmon resonance of large area bimetallic nanoparticle films by laser nanostructuring for chemical sensors, *Opt. Lett.* 36 (2011) 1362, <https://doi.org/10.1364/OL.36.001362>.
- [40] Y. Yang, Y. Peng, C. Lin, L. Long, J. Hu, J. He, H. Zeng, Z. Huang, Z.Y. Li, M. Tanemura, J. Shi, J.R. Lombardi, X. Luo, Human ACE2-functionalized gold “virus-trap” nanostructures for accurate capture of SARS-CoV-2 and single-virus SERS detection, *Nano Micro Lett.* 13 (2021) 109, <https://doi.org/10.1007/s40820-021-00620-8>.
- [41] Y. Yang, Z.Y. Li, K. Yamaguchi, M. Tanemura, Z. Huang, D. Jiang, Y. Chen, F. Zhou, M. Nogami, Controlled fabrication of silver nanoneedles array for SERS and their application in rapid detection of narcotics, *Nanoscale* 4 (2012) 2663, <https://doi.org/10.1039/c2nr12110g>.
- [42] S.B. Chaney, S. Shanmukh, R.A. Dluhy, Y.P. Zhao, Aligned silver nanorod arrays produce high sensitivity surface-enhanced Raman spectroscopy substrates, *Appl. Phys. Lett.* 87 (2005), 031908, <https://doi.org/10.1063/1.1988980>.
- [43] W. Zhang, Q. Tian, Z. Chen, C. Zhao, H. Chai, Q. Wu, W. Li, X. Chen, Y. Deng, Y. Song, Arrayed nanopore silver thin films for surface-enhanced Raman scattering, *RSC Adv.* 10 (2020) 23908–23915, <https://doi.org/10.1039/D0RA03803B>.
- [44] N.T. Panagiotopoulos, N. Kalfagiannis, K.C. Vasilopoulos, N. Pliatsikas, S. Kassavetis, G. Vourlias, M.A. Karakassides, P. Patsalas, Self-assembled plasmonic templates produced by microwave annealing: applications to surface-enhanced Raman scattering, *Nanotechnology* 26 (2015), 205603, <https://doi.org/10.1088/0957-4484/26/20/205603>.
- [45] C.A. Schneider, W.S. Rasband, K.W. Eliceiri, NIH image to ImageJ: 25 years of image analysis, *Nat. Methods.* 9 (2012) 671–675, <https://doi.org/10.1038/nmeth.2089>.
- [46] G. McNay, D. Eustace, W.E. Smith, K. Faulds, D. Graham, Surface-enhanced Raman scattering (SERS) and surface-enhanced resonance Raman scattering (SERRS): a review of applications, *Appl. Spectrosc.* 65 (2011) 825–837, <https://doi.org/10.1366/11-06365>.
- [47] R.D. Deegan, O. Bakajin, T.F. Dupont, G. Huber, S.R. Nagel, T.A. Witten, Capillary flow as the cause of ring stains from dried liquid drops, *Nature* 389 (1997) 827–829, <https://doi.org/10.1038/39827>.
- [48] K. Sefiane, Patterns from drying drops, *Adv. Colloid Interface Sci.* 206 (2014) 372–381, <https://doi.org/10.1016/j.cis.2013.05.002>.
- [49] R.D. Deegan, Pattern formation in drying drops, *Phys. Rev. E* 61 (2000) 475–485, <https://doi.org/10.1103/PhysRevE.61.475>.
- [50] P. Hildebrandt, M. Stockburger, Surface-enhanced resonance Raman spectroscopy of Rhodamine 6G adsorbed on colloidal silver, *J. Phys. Chem.* 88 (1984) 5935–5944, <https://doi.org/10.1021/j150668a038>.
- [51] N. Pliatsikas, G. Vourlias, P. Patsalas, Facile synthesis of tunable nanostructured plasmonic templates by electroless deposition, *Plasmonics* 13 (2018) 467–474, <https://doi.org/10.1007/s11468-017-0532-2>.
- [52] S. Lin, X. Lin, Y. Shang, S. Han, W. Hasi, L. Wang, Self-assembly of faceted gold nanocrystals for surface-enhanced Raman scattering application, *J. Phys. Chem. C* 123 (2019) 24714–24722, <https://doi.org/10.1021/acs.jpcc.9b06686>.
- [53] Y. Zhang, X. Chen, F. Liu, L. Li, J. Dai, T. Liu, Enhanced coffee-ring effect via substrate roughness in evaporation of colloidal droplets, *Adv. Condens. Matter Phys.* 2018 (2018) 1–9, <https://doi.org/10.1155/2018/9795654>.
- [54] D. Lohani, M.G. Basavaraj, D.K. Satapathy, S. Sarkar, Coupled effect of concentration, particle size and substrate morphology on the formation of coffee rings, *Colloids Surf. A Physicochem. Eng. Asp.* 589 (2020), 124387, <https://doi.org/10.1016/j.colsurfa.2019.124387>.
- [55] R. Sharma, M.S. Strano, Centerline placement and alignment of anisotropic nanotubes in high aspect ratio cylindrical droplets of nanometer diameter, *Adv. Mater.* 21 (2009) 60–65, <https://doi.org/10.1002/adma.200801287>.
- [56] A.G. Brolo, E. Arctander, C.J. Addison, Strong polarized enhanced Raman scattering via optical tunneling through random parallel nanostructures in Au thin films, *J. Phys. Chem. B* 109 (2005) 401–405, <https://doi.org/10.1021/jp046045u>.
- [57] Z.Q. Tian, Surface-enhanced Raman spectroscopy: advancements and applications, *J. Raman Spectrosc.* 36 (2005) 466–470, <https://doi.org/10.1002/jrs.1378>.
- [58] C.L. Haynes, R.P. Van Duyne, Plasmon-sampled surface-enhanced Raman excitation spectroscopy, *J. Phys. Chem. B* 107 (2003) 7426–7433, <https://doi.org/10.1021/jp027749b>.